

Chaos and ergodicity in entangled non-ideal Bohmian qubits

A.C. Tzemos *and G. Contopoulos

Research Center for Astronomy and Applied Mathematics of the
Academy of Athens - Soranou Efessiou 4, GR-11527 Athens,
Greece

March 7, 2022

Abstract

We study the Bohmian dynamics of a large class of bipartite systems of non-ideal qubit systems, by modifying the basic physical parameters of an ideal two-qubit system, made of coherent states of the quantum harmonic oscillator. First we study the case of coherent states with truncated energy levels and large amplitudes. Then we study non-truncated coherent states but with small amplitudes and finally a combination of the above cases. In all cases we find that the chaotic Bohmian trajectories are approximately ergodic. We also study the number and the spatial arrangement of the nodal points of the wavefunction and their role both in the formation of chaotic-ergodic trajectories, and in the emergence of ordered trajectories. Our results have strong implications on the dynamical establishment of Born's rule.

1 INTRODUCTION

In Bohmian Quantum Mechanics (BQM) the quantum particles evolve in space-time according to the so called Bohmian equations (BEs):

$$m_i \frac{dr_i}{dt} = \hbar \Im \left(\frac{\nabla_i \Psi}{\Psi} \right), \quad (1)$$

where Ψ is the wavefunction of the system under study [1, 2] and \Im stands for the imaginary part. The highly nonlinear character of the BEs allows the coexistence of chaotic and ordered trajectories, which have been studied extensively in the past [3, 4, 5, 6, 7, 8, 9, 10, 11, 12, 13, 14].

*Corresponding Author: atzemos@academyofathens.gr

The quantum harmonic oscillator (QHO) is the most studied quantum system. In BQM the 2-d and 3-d QHOs have been used extensively in the exploration of Bohmian chaos, since:

1. In the case of non-interacting quantum oscillators the corresponding Schrödinger equation is analytically solvable, i.e. we know with perfect accuracy the guiding wavefunctions of the Bohmian trajectories [15].
2. With a proper choice of their wavefunctions we can observe all possible kinds of Bohmian trajectories: ordered (periodic or not) and chaotic.

In fact, as it is well known from the very first studies in the field, the nodal points of the wavefunction play a key role for the production of chaotic Bohmian trajectories. According to the ‘so called nodal point-X-point complex (NPXPC) mechanism’ [13, 16], whenever a quantum particle comes close to a moving nodal point of the wavefunction Ψ it gets scattered by the so called X-point, a stagnant hyperbolic point in the frame of reference of the moving node. Every such scattering process is accompanied by a positive shift of the local Lyapunov characteristic number [17] and consequently contributes in the production of chaotic Bohmian trajectories. Trajectories that do not approach NPXPCs are ordered.

An important feature of the non-interacting QHOs is that, in many cases, we can find analytically the positions of the nodal points. This fact facilitates significantly all the calculations involved in the study of Bohmian chaos in most of our previous works.

A distinguished class of solutions of the quantum harmonic oscillator are the coherent states [18]. The coherent states are known as the minimum uncertainty states, which exhibit the closest possible behaviour to that of the classical harmonic oscillator. These states are of fundamental importance in Quantum Optics, since they describe under some conditions the state of a laser. Thus it is interesting to study their behaviour from a Bohmian standpoint.

In a series of previous works [19, 20, 21, 22] we used the coherent states of the QHO in order to construct qubits [23] and then studied in detail the Bohmian Dynamics of two such qubits for various degrees of quantum entanglement.

The two-qubit system with incommensurable frequencies ω_x and ω_y is convenient for both analytical and numerical calculations and has many interesting features:

1. It has infinitely many nodal points forming straight lines. The positions of the nodal points in time can be calculated analytically.
2. The infinite number of NPXPCs was found to be responsible for the production of chaotic-ergodic trajectories, for any non-zero entanglement (for zero entanglement (product states) there are no NPXPCs and all Bohmian trajectories are ordered). In fact we found that for any non-vanishing amount of the entanglement, the chaotic trajectories are essentially ergodic. The proportion of chaotic trajectories increases with entanglement and as we approach the maximum entanglement all trajectories become

chaotic-ergodic. Thus, for strongly entangled states almost any initial distribution with $P_0 \neq |\Psi_0|^2$ will finally reach the Born Rule (BR) distribution $P = |\Psi|^2$, since in these cases BR is dominated by chaotic-ergodic trajectories.

3. However, when the entanglement is weak the number of ordered trajectories in the Born distribution is significant. Therefore an arbitrary initial distribution will reach the Born distribution only if the ratio between its chaotic and ordered trajectories is approximately the same as that of the Born distribution.

The above results refer to a two-qubit model which consists of perfectly coherent states of two quantum harmonic oscillators in the x and y directions. But, as it is well known, a coherent state contains an infinite number of energy levels following a Poisson distribution around a mean value [18]. This infinite number of energies is responsible for the infinite number of the nodal points in this model, something crucial for the quick emergence of the ergodicity of the chaotic trajectories.

It is natural now to ask how general are our results i.e. what happens if we work with wavefunctions that deviate from a two-qubit model.

In the present paper we study the dynamics of generic bipartite Bohmian systems of quantum oscillators, by considering two basic modifications of the two-qubit model: a) coherent states with truncated energy levels and b) qubits with overlapping basis states.

The structure of the paper is the following: In section 2 we present the general form of the bipartite system of quantum harmonic oscillators and point out the key physical parameters. In section 3 we consider states with truncated energy levels in the two-qubit model and clarify the contribution of the various energy levels in the long time behaviour of the trajectories, for different values of the entanglement. Then in section 4 we compare our results with those of more general cases that deviate from a two-qubit system, namely: coherent states with common small amplitudes in x and y and coherent states with different amplitudes along the x and y axes. In section 5 we consider truncated coherent states with small amplitudes and finally, in section 6 we draw our conclusions.

2 A BIPARTITE SYSTEM OF QUANTUM HARMONIC OSCILLATORS

The coherent states of the 1-d quantum harmonic oscillator, corresponding to the classical system

$$H = \frac{1}{2}m\omega^2 x^2 + \frac{p^2}{2m}, \quad (2)$$

are defined as the eigenstates of the annihilation operator \hat{a} :

$$\hat{a}|\alpha\rangle = A|\alpha\rangle, \quad (3)$$

where the eigenvalue A is, in general, a complex number since \hat{a} is not hermitian, i.e. $A = |A| \exp(i\theta)$, where $|A|$ is the amplitude and θ the phase of the state $|\alpha\rangle$. The coherent states are written in the basis of Fock states as:

$$|\alpha\rangle = e^{-\frac{1}{2}|A|^2} \sum_{n=0}^{\infty} \frac{A^n}{\sqrt{n!}} |n\rangle, \quad (4)$$

where $|n\rangle$ are the eigenvectors of the Hamiltonian operator $\hat{H} = \hbar\omega(\hat{a}^\dagger\hat{a} + \frac{1}{2})$. The infinitely many energy eigenstates inside a coherent state follow Poissonian statistics [18], i.e. the probability of detecting energy level n in the state $|\alpha\rangle$ is

$$P(n) = |\langle n|\alpha\rangle|^2 = \frac{e^{-\langle n\rangle} \langle n\rangle^n}{n!}, \quad (5)$$

The mean value $\langle n\rangle$ and the variance $(\Delta n)^2$ are both constant, equal to $|A|^2$, and $\sum_{n=0}^{\infty} P(n) = 1$ (see Fig. 1). By taking the inner product $\langle x|\alpha\rangle$ and using the fact that the energies of the quantum harmonic oscillator are given by $E_n = \hbar\omega(n + \frac{1}{2})$, $n = 0, 1, 2, \dots$, one finds that the time dependent wavefunction of an 1-d coherent state is given by:

$$Y(x, t) = e^{-\frac{1}{2}a_0^2} e^{-\frac{i\omega_x t}{2}} \sum_{n=0}^{n_f} \frac{(a_0 e^{i\sigma_x} e^{-i\omega_x t})^n}{\sqrt{n!}} \psi_n(x), \quad (6)$$

where

$$\psi_n(x) = \frac{1}{\sqrt{2^n n!}} \left(\frac{m_x \omega_x}{\pi \hbar} \right)^{\frac{1}{4}} e^{-\frac{m_x \omega_x x^2}{2\hbar}} H_n \left(\sqrt{\frac{m_x \omega_x}{\hbar}} x \right), n = 0, 1, 2, \dots, \quad (7)$$

and $H_n(k) = (-1)^n e^{k^2} \frac{d^n}{dk^n} (e^{-k^2})$ are the corresponding Hermite polynomials. In the ideal coherent state we have $n_f = \infty$, while $a_0 = |A(0)|$, σ_x , ω_x are the initial values of the amplitude, the initial phase, and the frequency of the oscillator. Similarly there is an expression for $Y(y, t)$ with b_0, σ_y, ω_y instead of a_0, σ_x and ω_x . In our calculations we take $m_x = m_y = \hbar = 1$.

In our previous papers [19, 21, 20, 22], we studied the Bohmian Dynamics of entangled coherent states of the form

$$\Psi = c_1 Y_R(x, t) Y_L(y, t) + c_2 Y_L(x, t) Y_R(y, t), \quad (8)$$

where

$$Y_R(x, t) = Y(x, t; \sigma_x = 0), Y_L(x, t) = Y(x, t; \sigma_x = \pi) \quad (9)$$

and similarly for the coordinate y . In the limit of infinite energies $n_f = \infty$ and with $a_0 = b_0$ sufficiently large, Y_R and Y_L define the orthogonal basis states of a qubit, where Y_R (or Y_L) refers to a Gaussian blob of a coherent state starting at $t = 0$ on the right (or on the left) of the center of the oscillation. Consequently, with a proper choice of the coefficients c_1, c_2 for which we have

$|c_1|^2 + |c_2|^2 = 1$, the wavefunction Ψ describes a two-qubit model covering all the possible degrees of entanglement. We chose to work with real c_1, c_2 and used c_2 as the entanglement control parameter. For $c_2 = 0$ the entanglement is zero (product state) and for $c_2 = \sqrt{2}/2$ the entanglement is maximum (Bell state).¹

The key physical parameters for the qubit character of this model are a) the amplitudes of the oscillators: the larger the amplitudes the smaller the overlap between the two basis states of the qubits. b) the energy levels of the coherent state, which in the nontruncated case they are infinite. Thus, we first work with common large amplitudes $a_0 = b_0 = 2.5$ for both oscillators and truncate the energy levels n_f (section 3). Then we work with non-truncated states but with small amplitudes (section 4) and finally with truncated states and small amplitudes (section 5).

3 TRUNCATED COHERENT STATES

The energy levels inside the coherent states of every qubit follow a Poissonian distribution as the one shown in Fig. 1.

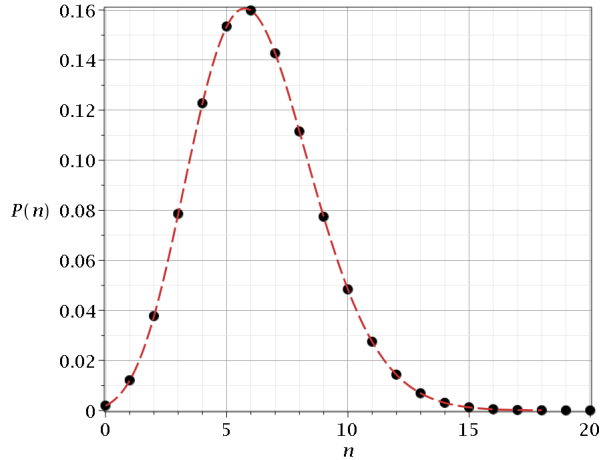


Figure 1: The energy level distribution $P(n)$ of a 1-d coherent state with $a_0 = 2.5$. In this case the average value of n is $\langle n \rangle = 6.25$.

We now study the case of truncated coherent states, where n_f is a finite positive integer. The non-classical properties of the truncated coherent states and their importance in Quantum Optics have already been studied in [24, 25, 26, 27]. Here we study the dynamics of the corresponding Bohmian trajectories. In these states the spectrum of the energies is smaller than the Poissonian one

¹In [19] we also considered wavefunctions of the form $\Phi = c_1 Y_R(x, t) Y_R(y, t) + c_2 Y_L(x, t) Y_L(y, t)$ but the results are qualitatively very similar to those of the case of Eq. 8.

of Fig. 1. In particular for $n_f = 2$ we cover only 5.1% of the total distribution, for $n_f = 4$ we cover 25.3% etc. In the maximum value that we consider in this paper, $n_f = 12$, we cover 98.7% of the full energy distribution and practically recover the full coherent state system.

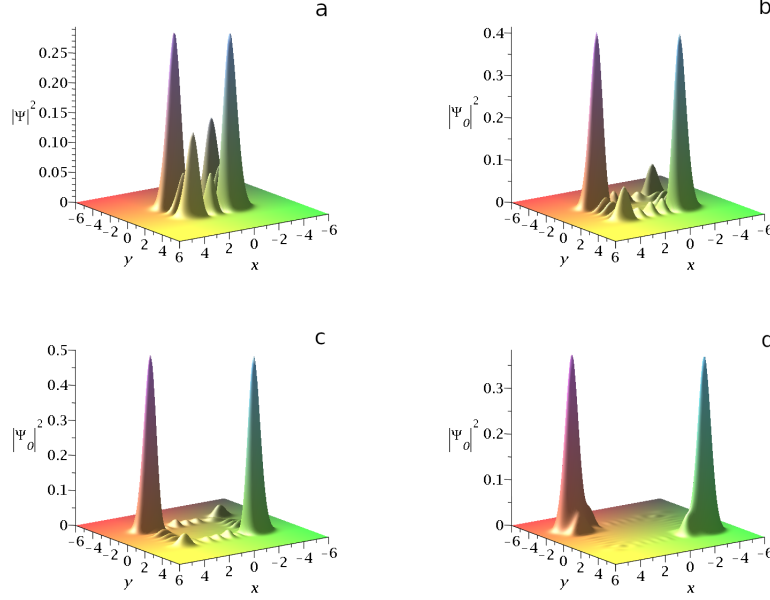


Figure 2: The initial probability density $P_0(x, y) = |\Psi_0|^2$ of the maximally entangled two-qubit state ($c_2 = \sqrt{2}/2$) with $a_0 = 2.5, \omega_x = 1, \omega_y = \sqrt{3}$, in truncated coherent states with a) $n_f = 2$, b) $n_f = 4$, c) $n_f = 6$ and d) $n_f = 10$. For $n_f \geq 12$ we recover the results of the full coherent state qubits (Fig. 1 of [21]).

First we calculate the normalized initial probability density $|\Psi_0|^2$ of finding a quantum particle at a certain point of the configuration space, which represents an initial particle distribution following the Born rule $P_0 = |\Psi_0|^2$. In Fig. 2 we show the case of the maximally entangled state ($c_2 = \sqrt{2}/2$) for various truncations. We observe two equal main blobs symmetric with respect to the origin. However, while for $n_f = \infty$ we have only these two blobs, when n_f is small we have a number of secondary blobs, which are relatively large for $n_f = 2$ and they become smaller as n_f increases. For $n_f > 10$ they practically disappear and we recover the probability density of the non-truncated case.

Furthermore we have nodal points when $\Psi_{Re} = \Psi_{Im} = 0$, whose number increases as n_f increases and tends to infinity as $n_f \rightarrow \infty$ and whose positions are aligned on a straight line when $n_f = \infty$ [22].

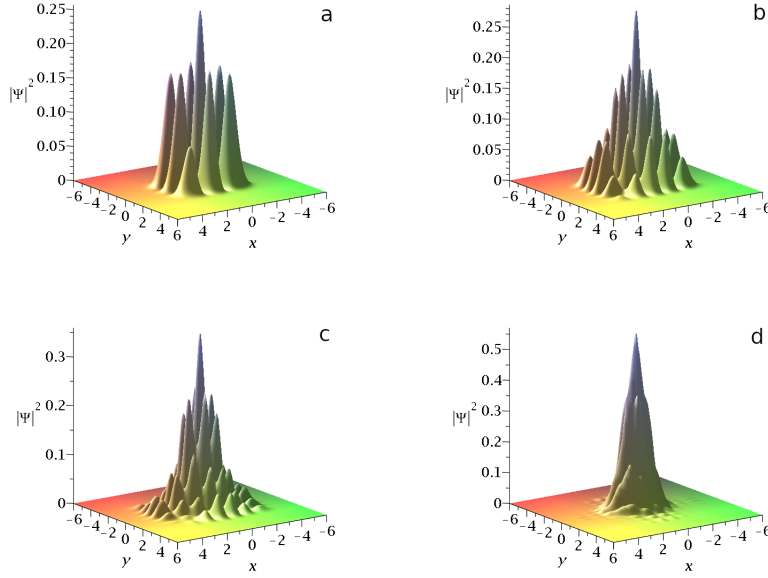


Figure 3: The probability density $P(x, y) = |\Psi|^2$ of the maximally entangled two-qubit state ($c_2 = \sqrt{2}/2$) with $a_0 = 2.5, \omega_x = 1, \omega_y = \sqrt{3}$ at $t = 4.58$, when the two main blobs collide, in truncated coherent states with a) $n_f = 2$, b) $n_f = 4$, c) $n_f = 6$ and d) $n_f = 10$.

At $t = 0$ the two blobs are at their maximum distance from the origin and, as the time increases, they move around the origin following approximately Lissajous figures (see Eq. 10)². The support of the wavefunction, i.e. the region where $|\Psi|^2$ is relatively large, is approximately a parallelogram around the origin (our plots cover the regions with $|\Psi|^2 \geq 10^{-5}$). At particular times the blobs collide close to the origin (Fig. 3). Such a collision appears for the first time at $t \simeq 4.58$ in all cases [20, 21] and they form a complicated pattern of secondary blobs for a small time interval. Between these blobs there are nodal points that scatter the particles of the blobs, so that all their trajectories become chaotic. After the collision the blobs are formed again and collide from time to time.

²We note that in the case of product states the Bohmian trajectories form exact Lissajous curves [19, 20].

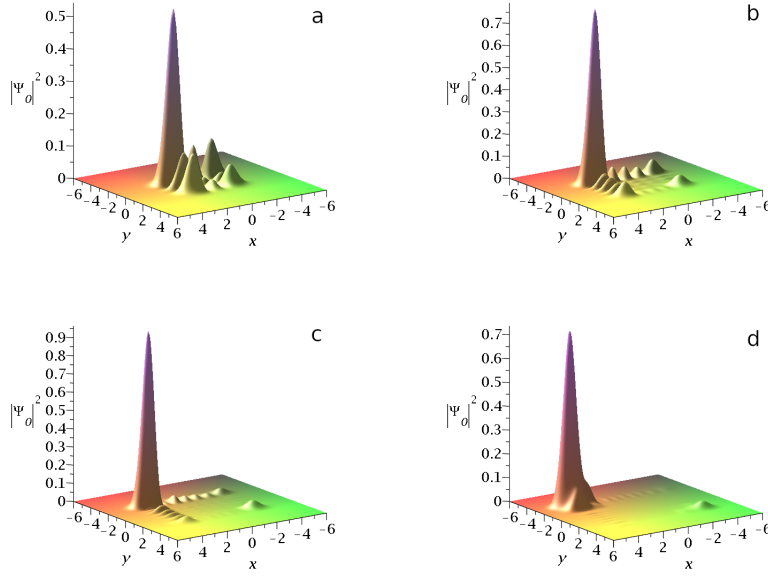


Figure 4: The initial probability density $P_0(x, y) = |\Psi_0|^2$ of a weakly entangled two-qubit state ($c_2 = 0.2$) with $a_0 = 2.5$, $\omega_x = 1$, $\omega_y = \sqrt{3}$, in truncated coherent states with (a) $n_f = 2$, (b) $n_f = 4$, (c) $n_f = 6$ and (d) $n_f = 10$.

On the other hand, we know from our previous works (e.g. [22]) that when c_2 is not maximum, the two main blobs are not equal. We found that the same holds for the small secondary blobs of the truncated cases: as c_2 decreases all initial blobs (main and secondary) of the fourth quadrant ($x > 0, y < 0$) become larger and those of the second quadrant ($x < 0, y > 0$) become smaller, as in the non-truncated system. E.g. the form of P_0 for $c_2 = 0.2$ and for various truncations is shown in Fig. 4.

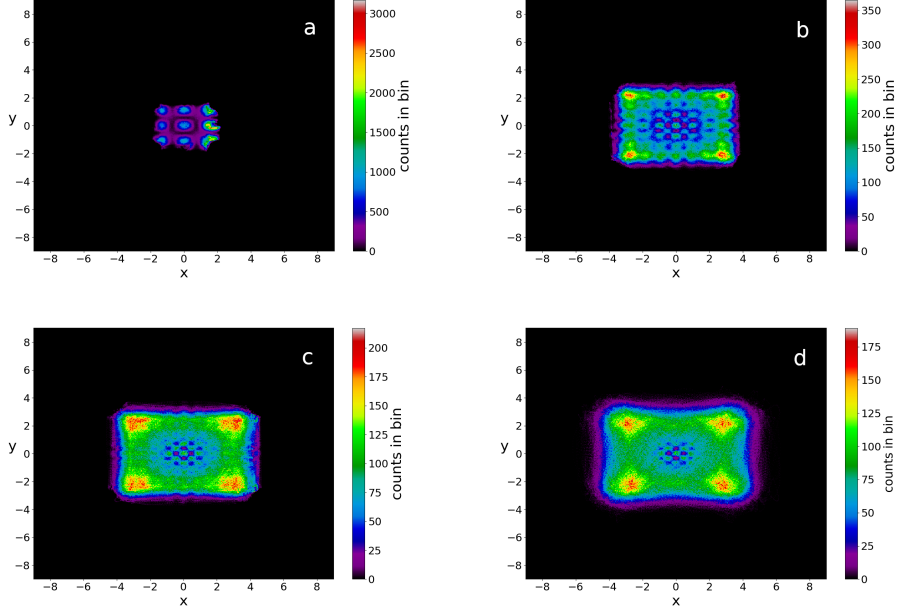


Figure 5: Maximally entangled state for (a) $n_f = 2$, (b) $n_f = 6$, (c) $n_f = 8$ and (d) $n_f = \infty$. We observe how the support of the wavefunction and consequently the range of motion, increases as $n_f \rightarrow \infty$.

Then we check the patterns of the limiting distributions of the points of the chaotic trajectories in various cases of the truncated states, using the methods developed in our previous papers [20, 21]. Namely, we make colorplots which depict how many times a trajectory has passed through the cells of a 360×360 square grid for $x, y \in [-9, 9]$ that covers the support of the wavefunction and compare the underlying arrays of the colorplots.

First we study the maximally entangled state ($c_2 = \sqrt{2}/2$). We compute the distribution of the points of a chaotic trajectory, taken at every $\Delta t = 0.05$ for times up to $t = 10^5$ and compare their pattern (Figs. 5a,b,c) with the corresponding distribution of the non-truncated system (Fig. 5d). We find that the distribution for $n_f = 2$ (Fig. 5a) is quite different from that for $n_f = \infty$ (Fig. 5d) and has a significantly reduced size in the configuration space, which corresponds to the size of the support of the truncated wavefunction³. In Fig. 5b we see that for $n_f = 6$ the size of the distribution is closer to that of the non-truncated state: their central parts, close to the origin look very similar and there exist four regions of high concentration close to the corners of the distribution. Finally, in Fig. 5c we see that for $n_f = 8$ we approach closely the

³In this model the chaotic trajectories cover in the long run all the support of the wavefunction. Therefore, the size of the distribution of points of a chaotic trajectory is essentially the same to the size of the support of Ψ .

$n_f = \infty$ distribution.

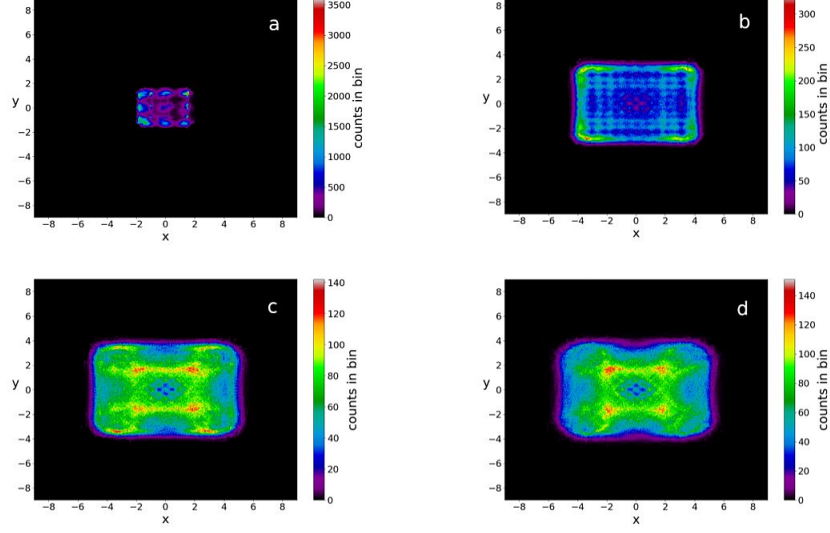


Figure 6: The trajectory with $x_0 = 0.1, y_0 = 0.4$ of the weakly entangled state $c_2 = 0.2$ up to $t = 10^5$ in the cases a) $n_f = 2$, b) $n_f = 8$, c) $n_f = 12$ and d) $n_f = \infty$.

Similar results appear in partially entangled states. E.g. the distribution of the points of a trajectory in the case $c_2 = 0.2$ approaches the coherent state distribution as n_f increases (Fig. 6). However, in this case the pattern of the final distribution of chaotic trajectories for $n_f = \infty$ (Fig. 6d) is different from that of Fig. 5d (smaller distances of the 4 regions of maximum concentration), as it was already shown in [21].

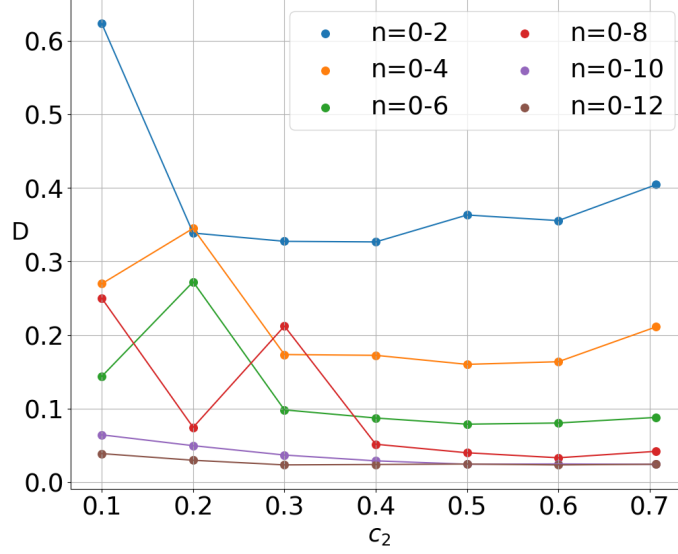


Figure 7: Frobenius distance between the final point distribution ($t = 10^5$) of a chaotic trajectory with initial conditions ($x_0 = 0.1, y_0 = 0.4$), for several ranges of energy levels (starting from $n = 0$) in the truncated coherent states and for given entanglements (c_2), from the corresponding complete coherent state.

These differences are established numerically by calculating the Frobenius norm [21, 22, 28] between the underlying matrices of the various color plots⁴. A detailed calculation is shown in Fig. 7, where we plot the distance of the pattern established after a time $t = 10^5$ between chaotic trajectories in the full coherent state and the truncated coherent states with $n_f = 2, 4, 6, 8, 10$ and 12, for various degrees of the entanglement.

We see that, for a given value of n_f , the values of D decrease in general, or remain roughly constant as the entanglement increases beyond the value $c_2 = 0.3$. On the other hand, for any given c_2 , D tends to zero as n_f increases. Thus we note that the main differences between the various patterns of points are due to the truncation order n_f and not to the entanglement. Namely the values of D for $n_f \geq 10$ become smaller than $D = 0.05$ for all the values of c_2 , and D becomes even smaller for larger n_f .

Furthermore, for every value of n_f and c_2 , we find that the Frobenius distance of two different chaotic trajectories is, in general, less than $D = 0.015$. Namely, the two trajectories reach practically the same limiting distribution of points.

⁴The Frobenius norm represents the distance between two matrices A, B and is equal to $\|A - B\| = \sqrt{\text{tr}[(A - B)^\dagger(A - B)]}$. We note that, in order to compare distributions by the same number of points we always divide the number of counts in the bins with the integration time.

In the case of maximum entanglement ($c_2 = \sqrt{2}/2$) all the trajectories inside the support of the wavefunction are chaotic and ergodic. Consequently, any arbitrary initial distribution of particles will reach in the long run the BR distribution, as in the case of the full coherent state system. However we note that there is a difference: in the non-truncated system we have infinite nodal points outside the support of the wavefunction, while for a small n_f there are only a few nodal points for every time t . Thus in the course of time there are large zones in the configuration space that do not contain nodal points (as we will see in Fig. 21a of section 5). This implies the possibility of the existence of ordered trajectories inside them. As n_f increases these zones are gradually filled with nodal points and in the limit $n_f \rightarrow \infty$ there are no ordered trajectories outside the support of the wavefunction. Consequently, in the maximally entangled state of truncated states with small n_f we have ordered trajectories but these are outside the support of the wavefunction, therefore they do not contribute significantly in the Born distribution. Thus Born's rule is accessible in the long run by all arbitrary initial distributions inside the support of the wavefunction, which is smaller than that of the non-truncated system.

On the other hand, for small c_2 we have ordered trajectories inside the support of the wavefunction, as in the non-truncated case, due to the different size of the blobs. Namely, the trajectories that start close to the top of the leading blob do not undergo scattering processes during the collisions of the blobs. This is due to the fact that the higher levels of the leading blob are practically unaffected by the collisions. Therefore for weakly entangled states Born's rule is accessible only by initial distributions with the same ratio between chaotic and ordered trajectories with the BR distribution, as in the non-truncated system.

The truncated coherent states deviate from Born's rule in the same way as in the case of the full coherent states considered in [21][20]. Namely, the chaotic trajectories of the truncated states for any value of the entanglement parameter c_2 are ergodic, but the patterns of their points are different from the patterns of the trajectories of the full coherent state. This difference decreases as n_f increases and tends to zero as n_f tends to infinity.

We have made similar calculations by truncating the coherent states not only from above (below $n_f = \infty$), but also from below (near $n_f = 0$).

This is shown in Fig. 8 where we have a figure similar to Fig. 7, but we have omitted the contributions of the low energy levels 0, 1, 2, 3, 4, 5. In this figure we gradually cover the range of high energies starting at $n_{in} = 6$ up to $n_f = 8, 10$, and 12 correspondingly. The general behaviour is similar to that of Fig. 7, namely: (a) as n_f increases the value of the Frobenius distance between the distribution of points of a chaotic trajectory in the truncated and the non-truncated case D decreases or remains almost constant beyond $c_2 = 0.3$. The limiting values of D for the same values of the upper n_f when $c_2 \rightarrow 0.707$ are about the same as in Fig. 7. (b) For a fixed value of c_2 the values of D for increasing n_f (upper) decrease in general and tend to zero.

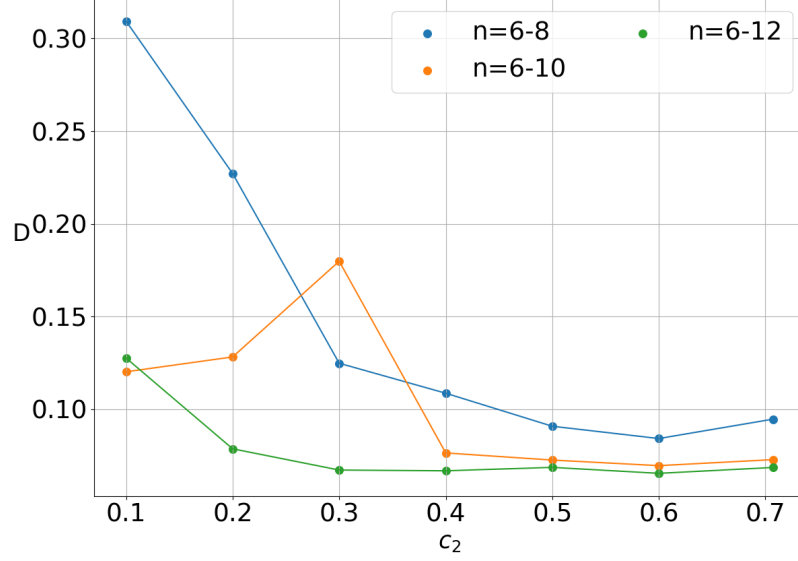


Figure 8: Frobenius distance between the distribution of points of a chaotic trajectory with $x_0 = 0.1, y_0 = 0.4$ of the truncated coherent states and the corresponding trajectory of the full qubit state for various degrees of entanglement (c_2).

4 COHERENT STATES WITH COMMON SMALL AMPLITUDES

A well known fact is that two arbitrary coherent states are not in general orthogonal, but have an interference which decreases with the increase of a_0 . Up to now we have used the value $a_0 = 2.5$ and we had a small interference of order 10^{-5} . On the other hand, if a_0 is small our model deviates from a two-qubit system, since we can not define the two basis states of the qubits.

In fact if a_0 is small there is an appreciable overlapping between the two coherent states, as shown in Fig. 9 for various values of a_0 and of the truncation order n_f . The overlap is given by the integral $\int_{-\infty}^{\infty} Y_L(x)Y_R(x)dx$. We observe the abrupt increase of the interference between Y_L and Y_R for $a_0 < 1.5$. In the case $a_0 = 1.0$ the qubit model breaks down completely.

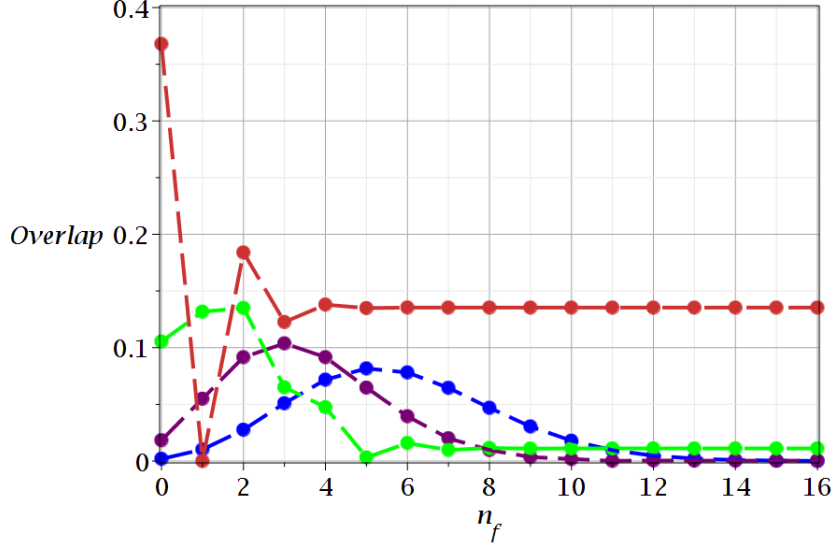


Figure 9: The overlap $\int_{-\infty}^{\infty} Y_L(x)Y_R(x)dx$ for various values of the truncation order n_f and for: $a_0 = 2.5$ (blue), $a_0 = 2.0$ (purple), $a_0 = 1.5$ (green), $a_0 = 1.0$ (red),

A small value of a_0 in the non-truncated system implies a small oscillation range for the Gaussian blobs around the origin. In fact the two blobs are formed around the points

$$x_c = \sqrt{\frac{2}{\omega_x}} a_0 \cos(\omega_x t), \quad y_c = \sqrt{\frac{2}{\omega_y}} a_0 \cos(\omega_y t) \quad (10)$$

and their maximum distances from the origin are

$$d_{max} = \frac{\sqrt{2(\omega_x + \omega_y)} a_0}{\sqrt{\omega_x \omega_y}}. \quad (11)$$

E.g. for $\omega_x = 1, \omega_y = \sqrt{3}$, we find $d_{max} \simeq 1.78 a_0$.

In Figs. 10 we plot the probability density $|\Psi|^2$ for $t = 0$ and $t = 4.58$ (collision time) of the maximally entangled ($c_2 = \sqrt{2}/2$) state when $a_0 = 2.5$ (top panel), $a_0 = 0.8$ (middle panel) and $a_0 = 0.5$ (bottom panel). The mean energy values in these cases are $a_0^2 = 6.25$, $a_0^2 = 0.64$ and $a_0^2 = 0.25$ correspondingly. As a_0 decreases the two blobs approach the origin (Figs. 10a,c) and for $a_0 = 0.5$ the two blobs have almost joined near the origin (Fig.10c). In the last case the two blobs overlap strongly and they can never be separated.

On the other hand the nodal points ($\Psi_{Real} = \Psi_{Imag} = 0$) are at the positions

$$\begin{aligned}
x_n &= \frac{\sqrt{2} \left(k\pi \cos(\omega_y t) + \sin(\omega_y t) \ln \left(\left| \frac{c_1}{c_2} \right| \right) \right)}{4\sqrt{\omega_x} a_0 \sin(\omega_{xy} t)}, \\
y_n &= \frac{\sqrt{2} \left(k\pi \cos(\omega_x t) + \sin(\omega_x t) \ln \left(\left| \frac{c_1}{c_2} \right| \right) \right)}{4\sqrt{\omega_y} a_0 \sin(\omega_{xy} t)},
\end{aligned} \tag{12}$$

with $k \in \mathbb{Z}$, k even for $c_1 \cdot c_2 < 0$ or odd for $c_1 \cdot c_2 > 0$, and $\omega_{xy} \equiv \omega_x - \omega_y$. For $c_1 = c_2$ their minimum distances from the center are:

$$d_n = \frac{\sqrt{2}\pi}{4a_0\sqrt{\omega_x\omega_y}\sin(\omega_{xy}t)} \sqrt{\omega_x \cos^2(\omega_x t) + \omega_y \cos^2(\omega_y t)} \tag{13}$$

When $t = 0$ the nodal points are at infinity, but during a collapse they approach the origin (Figs. 10b,d,f). The minimum values of d_n for $|k| = 1$ are given in Fig.11 and they are inversely proportional to a_0 .

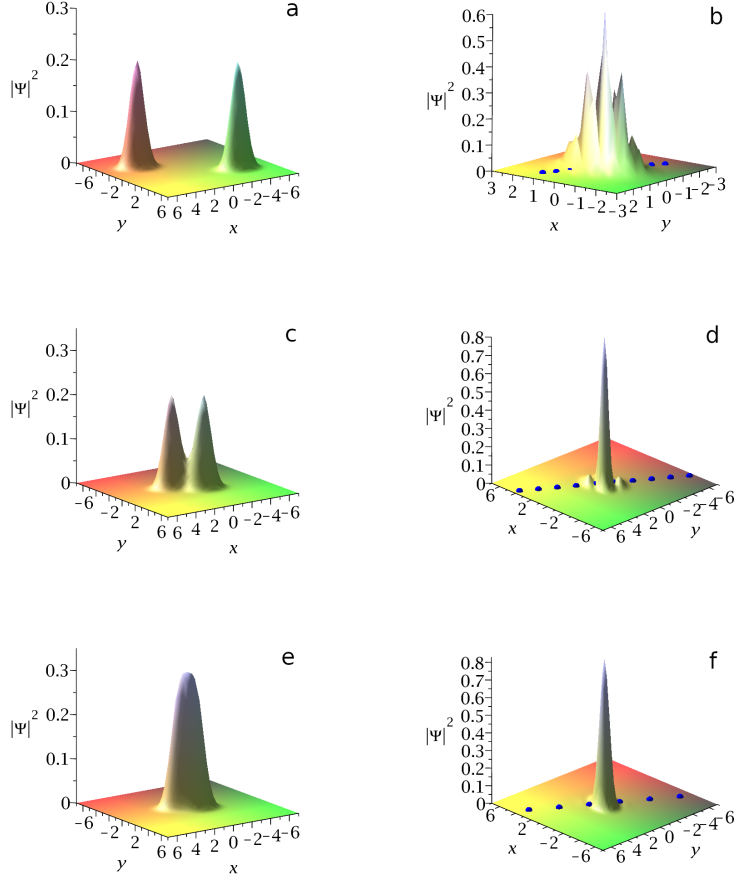


Figure 10: $|\Psi|^2$ in the case where $n_f = \infty$ and $a_0 = 2.5$ (top figures), $a_0 = 0.8$ (middle figures) and $a_0 = 0.5$ (bottom figures) for $t = 0$ and $t = 4.58$ (collision time). As a_0 decreases the nodal points move away from the central blob (the center of collision).

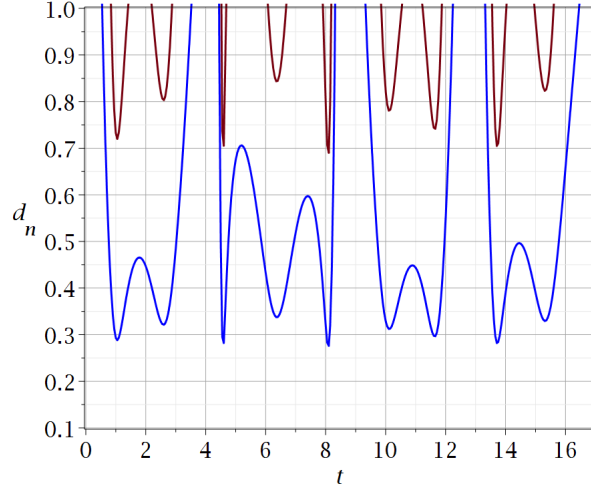


Figure 11: The distance between the origin and the nodal points $k = \pm 1$ as functions of time for $c_1 = c_2 = \sqrt{2}/2$, when $a_0 = 2.5$ (blue curve) and $a_0 = 1$ (burgundy curve). The greater the amplitude a_0 the smaller the distance d_n .

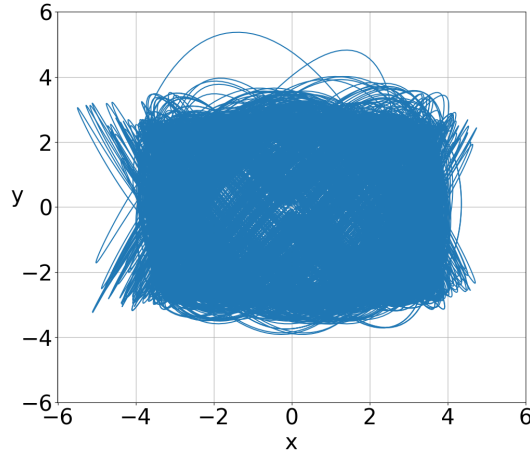


Figure 12: A typical chaotic trajectory in the case $a_0 = 2.5$ up to $t = 4000$ ($c_2 = \sqrt{2}/2, x_0 = 3, y_0 = 0$).

In the case $a_0 = 2.5$ the minimum values of d_n are about $d_n \simeq 0.3$, i.e. they are much smaller than the initial distances of the blobs from the center ($d_{max} = 10$). In general, for large a_0 the nodal points come closer to the origin than the tops of the two blobs during a collision, therefore they scatter the

trajectories close to the origin, which become chaotic. An example of such a chaotic trajectory is given in Fig. 12. However, for small a_0 the nodal points are outside the blobs and they do not produce chaotic trajectories near the center. In fact, the trajectories of the nodal points in the coherent state for $a_0 = 0.5$ leave empty a large area around the center (Fig. 13a) and further areas above, below and on the right and on the left. These empty regions are much larger in the case $a_0 = 0.5$ (Fig. 13a) than in the case $a_0 = 2.5$ (Fig. 13b). As a consequence, for $a_0 = 0.5$ the trajectories that start close to the origin ($d < 1$) do not approach any nodal point, therefore they are ordered. In Fig. 14 we see the areas covered by several ordered trajectories around the origin.

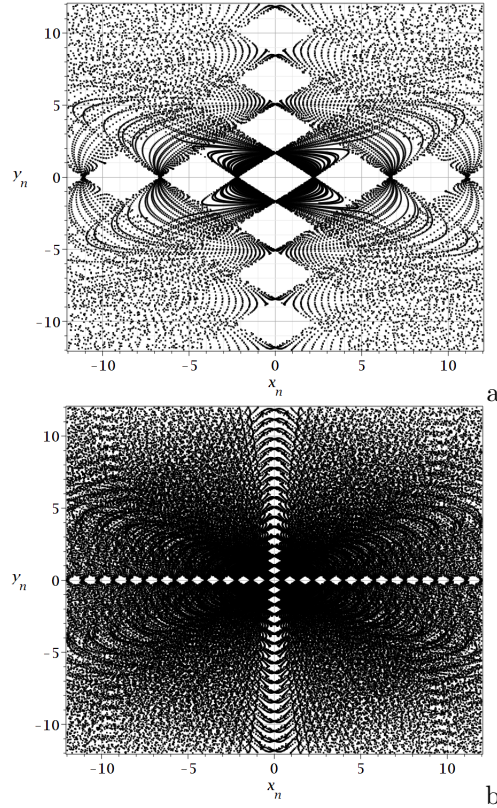


Figure 13: Nodal trajectories of the non-truncated system in the cases $a_0 = 0.5$ (a) and $a_0 = 2.5$ (b). The nodal trajectories have several empty regions which decrease as a_0 increases. For $a_0 \rightarrow \infty$ the empty regions practically disappear.

On the other hand, the trajectories starting further away from the origin are deflected by the NPXPCs and become chaotic. In Fig. 14 we see two chaotic trajectories. Each of them covers, after a time $t = 4 \times 10^5$, about half of a thick ring surrounding the origin. After a time $t = 7 \times 10^5$ both trajectories of Fig. 14

cover the whole ring (Fig. 15), but not in a uniform way. In fact, the points of the trajectories stay most of the time in rather small parts of the configuration space, although from time to time they cover the whole ring (Fig. 16a,b,c,d). That was verified for times up to $t = 10^7$.

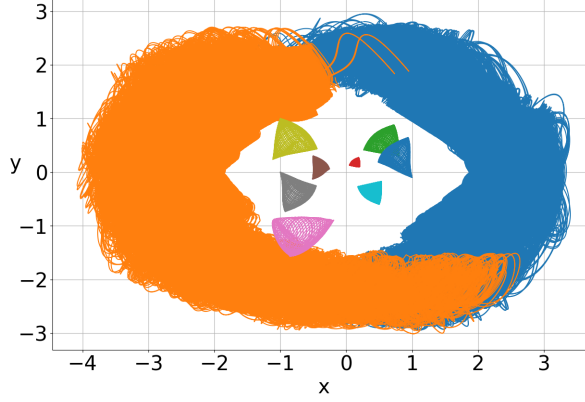


Figure 14: Bohmian trajectories of the full coherent state system in the case $a_0 = 0.5$. The chaotic trajectories are integrated up to $t = 4 \times 10^5$. We observe that the central region of the configuration space around the origin is now dominated by ordered trajectories (integrated up to $t = 200$). This is due to the fact that the nodal points do not enter in the central region.

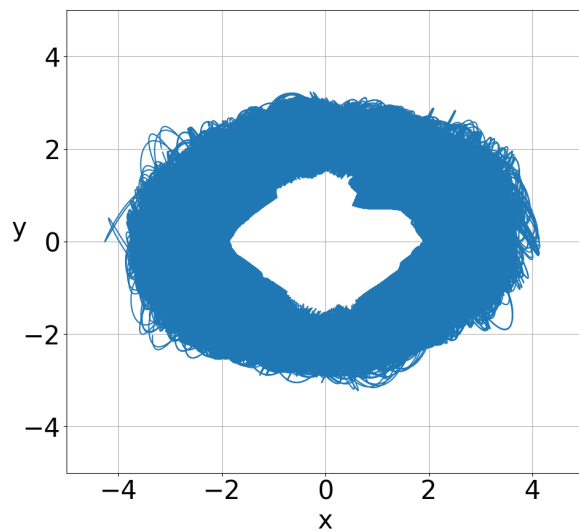


Figure 15: A chaotic trajectory $(x_0 = 3, y_0 = 0)$ covering a ring around the central blob of $|\Psi|^2$ in the case $a_0 = 0.5$, up to $t = 7 \times 10^5$.

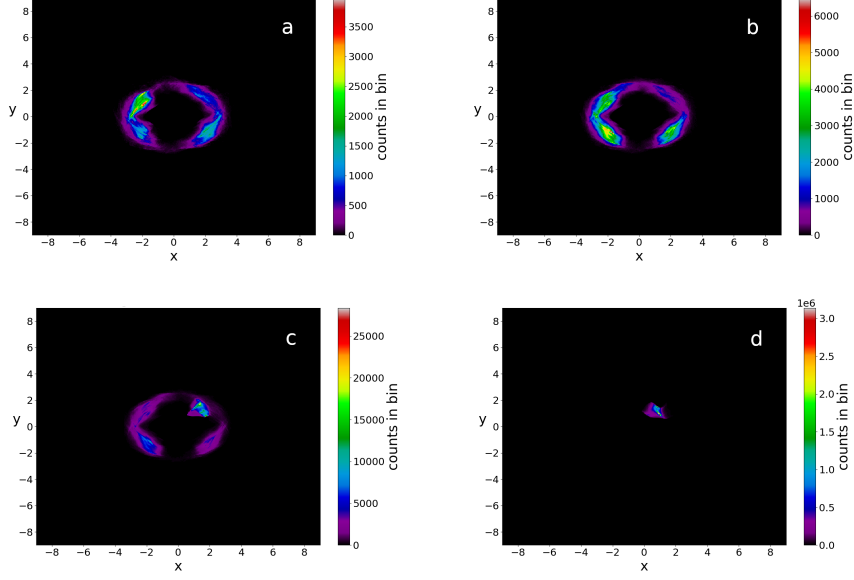


Figure 16: Successive colorplots of the points of the distribution of a chaotic trajectory $x_0 = 3, y_0 = 0$ in the case $a_0 = 0.5, c_2 = \sqrt{2}/2$ for a) $t = 200000$, b) $t = 400000$, c) $t = 600000$ and d) $t = 10^7$.

Therefore these trajectories do not appear to be ergodic for long times. This is also shown by calculating the Frobenius distance D between the distributions of the points of two such chaotic trajectories as a function of time (Fig. 17). However, a rough extrapolation of Fig. 17 shows that D approaches zero beyond $t = 4 \times 10^7$. Thus the chaotic trajectories become ergodic after an extremely long time.

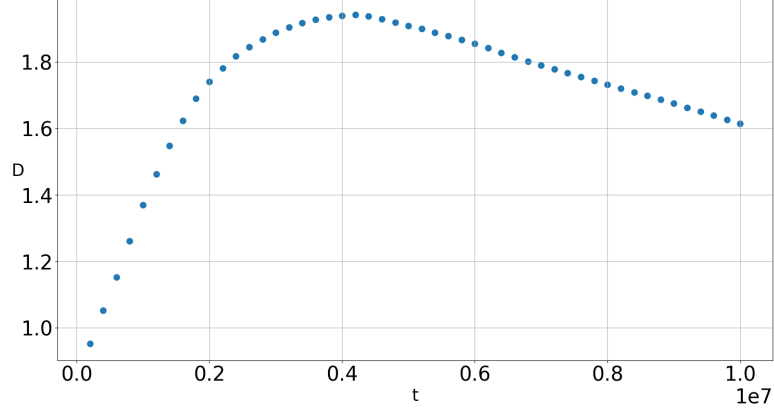


Figure 17: The Frobenius distance between two chaotic trajectories forming rings around the main blob, in the case $a_0 = 0.5$. D increases up to $t = 4 \times 10^6$. Only then it starts to decrease linearly in time with a power law, according to which D will reach zero at $t \simeq 4 \times 10^7$.

The problem now is how the trajectories for large a_0 (Fig. 12) transform to those of Fig. 14 with the decrease of the amplitude a_0 .

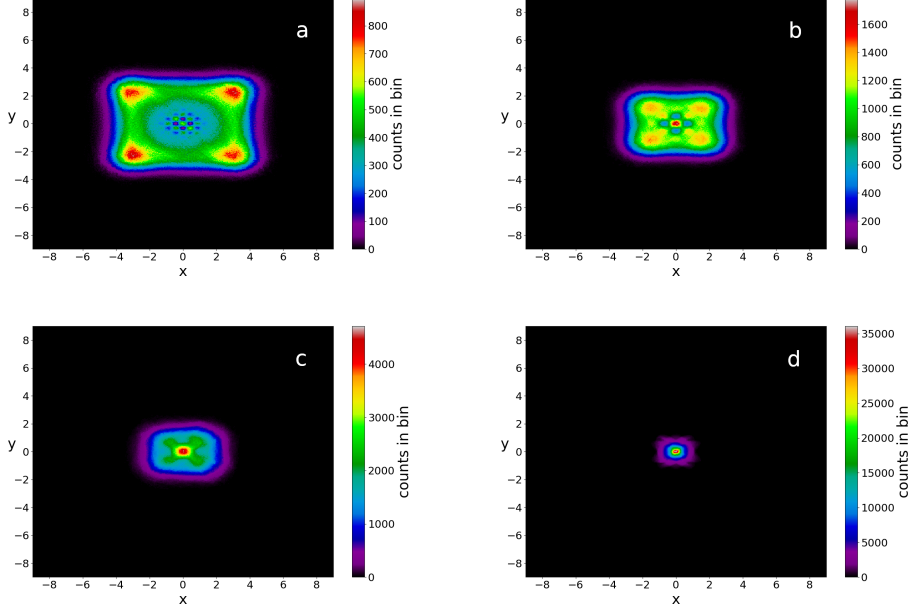


Figure 18: Colorplots of trajectories with the same initial conditions ($x_0 = 0.1, y_0 = 0.2$) in the maximally entangled state and for $t = 10^5$, when: (a) $a_0 = 2.5$, (b) $a_0 = 1.5$, (c) $a_0 = 1$ and (d) $a_0 = 0.8$. We observe how the 4 discrete blobs tend to join as a_0 decreases.

In Fig. 18 we construct the colorplots giving the distributions of the points of the chaotic trajectories, that start near the center of the configuration space. We observe that, for large a_0 , these plots form the usual pattern of four bright blobs near the corners of the support of the wavefunction (Fig. 18a). As a_0 decreases the distances of the bright blobs and the whole space distribution become smaller (Fig. 18b, c) and at the same time a maximum of density (red) appears at the center. For even smaller a_0 (Fig. 18d), the four blobs have joined the central maximum, which now dominates the distribution. However, the trajectories starting further away from the center form rings, as in the case of Fig. 15. As a_0 decreases the region near the center that contains regular trajectories becomes larger (Fig. 13).

Up to now we have considered coherent states with the same amplitudes a_0 along x and y coordinates. In Figs. 19a,b we consider the limiting distribution of the points of the trajectories in cases where the entanglement is maximum and the amplitude along x is $a_0 = 2.5$ but the amplitude along y is smaller, e.g. $b_0 = 0.5$ (Fig. 19a) and $b_0 = 1$ (Fig. 19b). By comparison with the non-truncated qubit case $a_0 = b_0 = 2.5$ (Fig. 18a), we observe that, as b_0 decreases, the pattern becomes more concentrated close to the x -axis. In particular, in Fig. 19b the two upper maxima of the probability density come closer to the

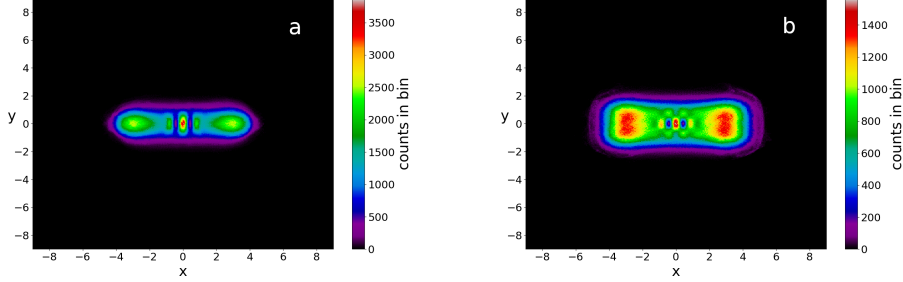


Figure 19: Colorplots of trajectories with the same initial conditions ($x_0 = 0.1, y_0 = 0.2$) in the maximum entangled state and up to $t = 10^5$ for $a_0 = 2.5$ and (a) $b_0 = 0.5$, (b) $b_0 = 1$.

lower maxima (in comparison with Fig. 18a), and in Fig. 19a the upper and the lower maxima have practically joined, so that we have only two maxima, one on the left and one on the right. On the other hand, the distances between the maxima along the x -axis remain about the same. We have checked numerically that all the chaotic trajectories are ergodic and their number increases with entanglement, as in the case with common amplitudes.

5 TRUNCATED COHERENT STATES WITH SMALL AMPLITUDES

In the cases where the amplitudes are small, we saw that the probability density is dominated by a central blob whose motion is confined very close to the origin.

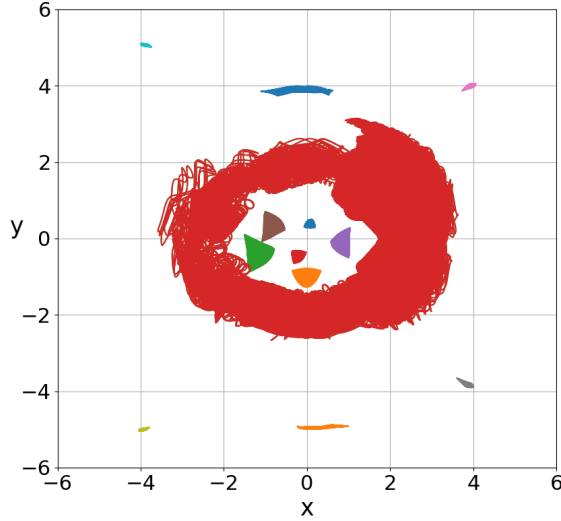


Figure 20: Several ordered trajectories in the truncated case with $a_0 = b_0 = 0.5$ inside and outside the support (approximately $x \in [-1.85, 1.85]$ and $y \in [-1.5, 1.5]$), when the truncation is $n_f = 2$ for times up to $t = 200$. We also show a typical chaotic trajectory surrounding the support of the wavefunction for times up to $t = 4 \times 10^5$.

Thus we expect that even with a truncated wavefunction we will find mostly ordered trajectories in that region, as shown in Fig. 20. These trajectories are of different forms, but they all have zero Lyapunov characteristic number [17]. There are also many chaotic trajectories around the central blob of the probability density $|\Psi|^2$ which form rings around the central blob, as the red trajectory of Fig. 20. These trajectories surround the support of Ψ , whose extent is approximately equal to the central hole of Fig. 20. However, due to the truncation of the energy levels, i.e. the finite number of nodes, we find also ordered trajectories further outside the support of the wavefunction. This is the basic difference between the truncated and the non truncated case, where all the ordered trajectories are inside the support of Ψ [22].

We must note that, for a detailed study of ordered and chaotic Bohmian trajectories, one needs to compute the trajectories of the nodal points. However, it is not possible, in general, to solve analytically the algebraic equations defining the positions of the nodal points in the truncated cases, which are of degree $2n_f$. Thus we are obliged to find these points numerically. This calculation is difficult when the various nodal points approach each other and when their velocities become large (when they go to or come from infinity).

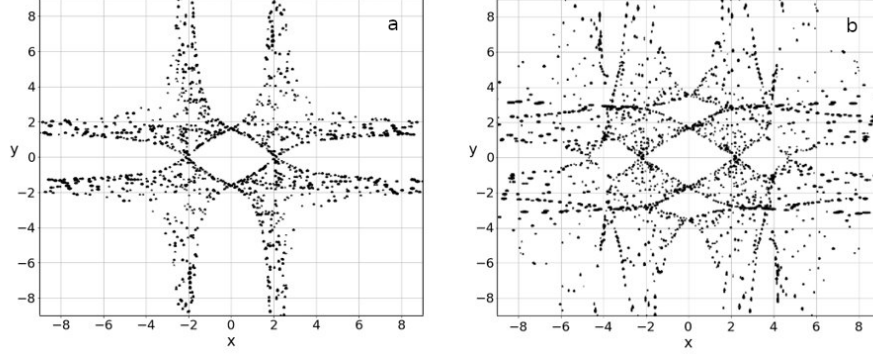


Figure 21: The dots represent the very small contour plots around the nodal points in the case where $a_0 = b_0 = 0.5$, for $t \in [0, 100]$ with time step $\Delta t = 0.01$ and $n_f = 2$ (a), and for $t \in [0, 50]$ and $n_f = 4$, with time step $\Delta t = 0.025$ (b).

Nevertheless, we managed to make a graphical depiction of the nodal points of the truncated coherent states by use of contour plots. Namely, in Fig. 21 we exploit the fact that the velocity of a Bohmian particle becomes extremely large as we approach the nodal points, and plot the contour plots of the Bohmian flow when the velocity is very high ($|v| = 500$). These contours are very small closed curves around the nodal points. This graphical method is, of course general (i.e. works for every wavefunction) and is useful since it gives approximately the positions of the nodes in the configuration space for any time. In Figs. 21a,b we show the contour plots in cases with $a_0 = b_0 = 0.5$ and $n_f = 2$ up to time $t = 100$ with time step $\Delta t = 0.01$ (Fig. 21a) and $n_f = 4$ up to time $t = 50$ with time step $\Delta t = 0.025$ (Fig. 21b).⁵

In the case $n_f = 2$ we have four nodal points whose distribution leaves extended empty regions in the configuration space. In the case $n_f = 4$ we have eight nodal points and their distribution covers many empty regions of the case $n_f = 2$. As n_f increases the empty regions tend to take the form of Fig. 13a.

A limiting case of a system in which the values of n are truncated from above and below so that only one value remains along x (n_x) and y (n_y) is the wavefunction $Y_{n_x, n_y}(x, y, t) = Y_{n_x}(x, t)Y_{n_y}(y, t)$. However if we have a sum of such terms $\Psi(x, y, t) = \sum_{n_x, n_y} c_{n_x, n_y} Y_{n_x, n_y}(x, y, t)$ we have in general both chaos and order. Such cases were considered in our previous papers [9, 10] and they are similar to the cases considered in the present section. In particular, Figs. 3 of [9, 10] are similar to the present Fig. 21a.

⁵As the truncation energy corresponding to n_f increases the time of the calculation of these figures increases significantly due to the high degree of the polynomials involved in the wavefunction.

6 CONCLUSIONS

We study the interplay between order and chaos in representative cases of bipartite Bohmian systems, and its implications on the dynamical establishment of Born's rule by an arbitrary initial distribution of Bohmian particles.

In previous papers we considered the case of two qubits with a wavefunction of the generic form $\Psi = c_1 Y_R(x, t) Y_L(y, t) + c_2 Y_L(x, t) Y_R(y, t)$ ($|c_1|^2 + |c_2|^2 = 1$), which covers all the range of entanglements, from zero up to maximum entanglement. These qubits are represented by coherent states of two non-interacting quantum harmonic oscillators. The infinite number of energy levels inside the Poisson distribution of the coherent states implied the existence of infinitely many NPXPCs, which scatter the incoming trajectories and produce chaos. The probability density $|\Psi|^2$ of this model is characterized by two Gaussian blobs which move in the configuration space and collide from time to time [21, 20]. The sizes of these blobs depend on the degree of the entanglement.

The chaotic trajectories of this model were found to be essentially ergodic for any non-zero entanglement, while their number increases with the entanglement. In fact, we found that in the maximally entangled state ($c_2 = c_1 = \sqrt{2}/2$) all the trajectories are chaotic and ergodic. Then any initial distribution of such trajectories will finally approach Born's rule ($P = |\Psi|^2$) after a long time. However, when the entanglement is small there are also ordered trajectories close to the center of the leading blob. Thus Born's rule is not accessible if the initial distribution does not contain approximately the same proportion of ordered and chaotic trajectories with that of the Born distribution.

In the present paper we study various cases that deviate from the two-qubit model by changing in many ways the physical parameters of the basis states of the qubits. The two major modifications we consider are:

1. The truncation of the coherent states which compose the qubits, at various energy levels for large amplitudes. From a Bohmian perspective this means that we worked with a finite number of NPXPCs. By plotting the long limit distributions of various truncations and by numerically calculating the motion of the nodal points in two truncated cases we observed the contribution of the various energies in the long limit dynamics of the ideal two-qubit system. When the number of nodal points is small, the patterns produced by the distribution of the points of the trajectories are different from the pattern of the full state, but as the number of the nodal points increases the patterns approach the pattern of the non-truncated system.

In the truncated cases we find that besides the two main blobs of $|\Psi|^2$ there are also several secondary blobs for all times (and not only during collisions). Moreover we find ordered trajectories, not only close to the center of the leading blob, but also outside the support of the wavefunction, even in the maximum entanglement case.

On the other hand the chaotic trajectories are still approximately ergodic even for low energies. This is due to the fact that, as the energy decreases, the size of the support of the wavefunction also decreases. Thus,

most chaotic trajectories evolve in a confined region around the origin and their close encounters with the NPXPCs lead to the same (approximately) limiting distribution. Consequently, the Born rule is accessible in the long run, only if the initial distribution has the correct ratio between chaotic and ordered trajectories inside the support of the wavefunction.

2. Then we considered coherent states with small amplitudes (a_0) for maximum entanglement. In these cases there are also infinite nodal points but they do not come very close to the origin as in the case of large amplitudes. As a consequence the trajectories close to the origin are ordered. Further away we find chaotic trajectories which fill a thick ring around the origin. The distribution of the points in this ring is irregular for long times but it seems to become uniform after an extremely long time. Therefore these trajectories are probably ergodic in the limit $t \rightarrow \infty$. These trajectories evolve on the outer part of the distribution of the probability density $|\Psi|^2$ and their number is small in the Born distribution, in contrast with the maximally entangled case of large a_0 where chaotic-ergodic trajectories dominate the Born distribution and cover all the support of the wavefunction. We studied in detail the transition from large to small common amplitudes which imply deviations from the two-qubit model. Similar results were found in the case of different amplitudes in x and y directions, where for large a_0 and small b_0 we observed that the distribution of the points of the trajectories are concentrated close to the x -axis.
3. Finally we studied truncated cases with small amplitudes. These cases have both order and chaos and are similar to cases studied in previous works of ours [9, 10], where the wavefunction was of the form $\Psi(x, y, t) = \sum_{n_x, n_y} c_{n_x, n_y} Y_{n_x}(x, t) Y_{n_y}(y, t)$. By developing a general way to depict graphically the positions of the nodal points of the truncated wavefunction when we do not have their analytical formulae, we found that in the cases with small amplitudes, there are ordered trajectories not only inside the support of the wavefunction (as in the non truncated system) but also at large distances from this support.

In all the aforementioned cases we have considered solutions of Schrödinger's equation corresponding to two harmonic oscillators with non-commensurable frequencies. In these cases we find in general both chaotic and ordered trajectories. When the frequencies are commensurable all the trajectories are periodic [19] and therefore there is no chaos at all.

We must emphasize here that all the cases considered above refer to a 2-d system of non-interacting harmonic oscillators. Thus it would be interesting to extend our studies:

1. In higher dimensional systems (multipartite systems) In particular, we have already shown that in the case of 3 ideal qubits, the increase of the dimensionality of the system implies an increase of the number of the chaotic states for any non zero entanglement. Thus in multiqubit systems

with $n \gg 3$ we expect that Born's rule is going to be reached practically by any initial distribution of particles [29] .

2. In more general Hamiltonians with interaction terms, as e.g. in the case of the quantum Hénon-Heiles model considered in [7].

Acknowledgements

This research was conducted in the framework of the program of the RCAAM of the Academy of Athens "Study of the dynamical evolution of the entanglement and coherence in quantum systems."

References

- [1] D. Bohm, A suggested interpretation of the quantum theory in terms of "hidden" variables. i, Phys. Rev. 85 (1952) 166.
- [2] D. Bohm, A suggested interpretation of the quantum theory in terms of "hidden" variables. ii, Phys. Rev. 85 (1952) 180.
- [3] G. Iacomelli, M. Pettini, Regular and chaotic quantum motions, Phys. Lett. A 212 (1) (1996) 29–38.
- [4] H. Frisk, Properties of the trajectories in Bohmian mechanics, Phys. Lett. A 227 (3-4) (1997) 139–142.
- [5] P. Falsaperla, G. Fonte, On the motion of a single particle near a nodal line in the de broglie–Bohm interpretation of Quantum Mechanics, Phys. Lett. A 316 (6) (2003) 382–390.
- [6] D. A. Wisniacki, E. R. Pujals, Motion of vortices implies chaos in Bohmian Mechanics, Europhys. Lett. 71 (2) (2005) 159.
- [7] C. Efthymiopoulos, G. Contopoulos, Chaos in Bohmian Quantum mechanics, J. Phys. A 39 (8) (2006) 1819.
- [8] D. Wisniacki, E. Pujals, F. Borondo, Vortex dynamics and their interactions in quantum trajectories, J. Phys. A 40 (48) (2007) 14353.
- [9] C. Efthymiopoulos, C. Kalapotharakos, G. Contopoulos, Nodal points and the transition from ordered to chaotic Bohmian trajectories, J. Phys. A 40 (43) (2007) 12945.
- [10] G. Contopoulos, C. Efthymiopoulos, Ordered and chaotic Bohmian trajectories, Celest. Mech. Dyn. Astron. 102 (1-3) (2008) 219–239.
- [11] G. Contopoulos, C. Efthymiopoulos, M. Harsoula, Order and chaos in Quantum Mechanics, Nonlin. Phen Comp. Sys. 11 (2) (2008) 107–120.

- [12] F. Borondo, A. Luque, J. Villanueva, D. A. Wisniacki, A dynamical systems approach to Bohmian trajectories in a 2d harmonic oscillator, *J. Phys. A* 42 (49) (2009) 495103.
- [13] C. Efthymiopoulos, C. Kalapotharakos, G. Contopoulos, Origin of chaos near critical points of quantum flow, *Phys. Rev. E* 79 (2009) 036203.
- [14] G. Contopoulos, N. Delis, C. Efthymiopoulos, Order in de Broglie–Bohm quantum mechanics, *J. Phys. A* 45 (16) (2012) 165301.
- [15] L. E. Ballentine, *Quantum Mechanics: a Modern Development*, World Scientific Publishing Company, 2014.
- [16] A. C. Tzemos, C. Efthymiopoulos, G. Contopoulos, Origin of chaos near three-dimensional quantum vortices: A general Bohmian theory, *Phys. Rev. E* 97 (4) (2018) 042201.
- [17] G. Contopoulos, *Order and Chaos in Dynamical Astronomy*, Springer, 2002.
- [18] J. Garrison, R. Chiao, *Quantum Optics*, Oxford University Press, 2008.
- [19] A. C. Tzemos, G. Contopoulos, C. Efthymiopoulos, Bohmian trajectories in an entangled two-qubit system, *Phys. Scr.* 94 (2019) 105218.
- [20] A. C. Tzemos, G. Contopoulos, Ergodicity and Born’s rule in an entangled two-qubit Bohmian system, *Phys. Rev. E* 102 (4) (2020) 042205.
- [21] A. C. Tzemos, G. Contopoulos, Chaos and ergodicity in an entangled two-qubit Bohmian system, *Phys. Scr.* 95 (6) (2020) 065225.
- [22] A. Tzemos, G. Contopoulos, The role of chaotic and ordered trajectories in establishing Born’s rule, *Phys. Scr.* 96 (6) (2021) 065209.
- [23] J. Asbóth, P. Adam, M. Koniorczyk, J. Janszky, Coherent-state qubits: entanglement and decoherence, *Eur. Phys. J. D* 30 (3) (2004) 403–410.
- [24] W. S. Chung, Even and odd truncated coherent states and their nonclassical properties, *Int. J. Mod. Phys. B* 28 (28) (2014) 1450194.
- [25] S. Sivakumar, Truncated coherent states and photon-addition, *Int. J. Theor. Phys.* 53 (5) (2014) 1697–1709.
- [26] W. S. Chung, H. Hassanabadi, Two mode superposition of truncated coherent states: Entanglement and non-classical properties, *Int. J. Theor. Phys.* 59 (4) (2020) 1069–1080.
- [27] W. S. Chung, H. Hassanabadi, Truncated exponential polynomials and truncated coherent states, *Eur. Phys. J. Plus* 135 (7) (2020) 1–11.
- [28] G. Strang, *Introduction to Linear Algebra*, Wellesley-Cambridge Press, 1993.

- [29] A. C. Tzemos, G. Contopoulos, Ergodicity and Born's rule in an entangled three-qubit Bohmian system, *Phys. Rev. E* 104 (5) (2021) 054211.